Photoinduced Formation of Selenium Molecules in Zeolites: A Resonant Raman Spectroscopy Study

A. Goldbach, M. Grimsditch, L. Iton, and Marie-Louise Saboungi*

Materials Science Division, Argonne National Laboratory, Argonne, Illinois 60439

Received: August 20, 1996; In Final Form: November 4, 1996[⊗]

After excitation of selenium encapsulated in Y-zeolite with 476 nm radiation, decomposition of the initially present semiconductor chains is observed. The fragmentation is influenced by the nature of the cations that counterbalance the negative charges of the aluminosilicate framework of the zeolite. In La^{3+}- and Nd^{3+}-exchanged Y-zeolite, Se_2^- is formed upon irradiation with 476 nm laser light while Se_3 is generated in the Ca^{2+}-exchanged form under the same conditions. Both species are identified by their resonance Raman spectra. The vibrational constants obtained for the electronic ground state of Se_3 in Ca-Y are $\omega_0 = 315$ cm^{-1} and $\omega_0 x_0 = 0.5$ cm^{-1}, the respective values for Se_2^- in La-Y are $\omega_0 = 329$ cm^{-1} and $\omega_0 x_0 = 0.8$ cm^{-1}.

Introduction

Recently we reported the formation of the Se_2^- radical anion in a Se-loaded Nd-Y zeolite under illumination with 476 nm laser radiation.[1] Although there have been a number of earlier studies on Se-loaded molecular sieves involving the illumination of the materials with radiation sufficiently high in energy to bridge the band gap of the incorporated semiconductor, no evidence of a photoinduced generation of small molecular Se species was given. Katayama et al. studied photoinduced phenomena in isolated Se chains encapsulated in mordenite between 30 K and room temperature.[2] They reported the appearance of new absorption bands upon illumination at low temperatures. These bands were associated with paramagnetic defects, and it has been suggested that these paramagnetic centers are neutral dangling bond sites with unpaired spin.[3] Both phenomena disappear by annealing the samples at room temperature. In contrast, Se_2^- is preserved in Nd-Y at room temperature.[1]

Bogomolov et al.[4−7] and Poborchii[8,9] undertook several Raman spectroscopic studies on selenium incorporated in different zeolites. Although they employed laser energies high enough for electronic excitation of the incorporated Se, fragmentation of the isolated chain and ring structures was not reported. On the other hand, it is known that Se_2^- is the chromophore in red selenium ultramarine which is an aluminosilicate of the feldspathoid family.[10] The stabilization of Se_2^- in the sodalite cages of ultramarine may bear resemblance to the stabilization of Se_2^- in the supercages of Y-zeolite. However, in selenium ultramarine, Se_2^- forms in the course of the crystallization of this synthetic mineral at high temperatures.[11]

In our earlier paper[1] on Se_2^- in Nd-Y we explained the formation of the radical anion from Se_2 involving $Nd_xO_y(OH)_z^{n+}$ clusters which are known to form in Y zeolites. Although these clusters include paramagnetic Nd^{3+} cations, the tendency of Nd^{3+} itself to transfer an electron and form Nd^{4+} is low. Hence, we suggested that the reducing power of the Nd-Y zeolite lies in the presence of hydroxyl-bridged clusters. Here we present investigations on the role of La^{3+} and Ca^{2+} in the formation of Se molecules in Y zeolites. Similarly to Nd^{3+} the closed-shell La^{3+} ion forms hydroxyl-bridged clusters inside Y zeolite[12,13] while Ca^{2+} ions are separately bound by the zeolite framework as single unbridged cations.

Experimental Section

The general procedure of the sample preparation has been described previously.[1] The countercations are introduced into the zeolite by a twofold ion exchange of Na-Y in aqueous La-$(CH_3CO_2)_3$ or $CaCl_2$ solution, respectively. Subsequently the zeolites are treated with oxygen to remove hydrocarbon impurities and dehydrated under vacuum at 550 °C. Finally, weighted amounts of the zeolite and selenium (separated by a frit) are loaded into a quartz U-tube inside a drybox. After both ends are sealed off under vacuum, the tube is heated to 350°C for several days. The resulting material has a homogeneously orange color. The selenium (calculated for maximum Se loading of the zeolites) is absorbed completely according to the weight balance yielding a Se weight fraction of 0.34 for La-Y and 0.37 for Ca-Y. This corresponds to approximately 13 Se atoms per supercage for both zeolites, which we have found to be the experimental upper limit for absorption of Se into Y zeolite by our method. Note that under pressure and using molten Se up to 21 Se atoms can be encapsulated in the supercages of zeolite X.[6,14] In what follows we refer to our materials as La-Y/13.5Se and Ca-Y/12.5Se, respectively.

The effects of the irradiation were examined by Raman spectroscopy at room temperature. The experimental setup consisted of a krypton ion laser and a triple Jobin Yvon T64000 spectrometer equipped with an optical multichannel analyzer. The resolution of the instrument was set to 6 cm^{-1}. For excitation we used the 476.2 and 647.1 nm laser lines, and the samples were contained in quartz tubes sealed under vacuum. Since the spectral range of the CCD detection system was limited to 350 cm^{-1} at 647.1 nm and 750 cm^{-1} at 476.2 nm, spectra extending over a wider range were generated as composites of single spectra in the previously described way.[1]

Results

Depending on the wavelength and power used for excitation, different Raman spectra were observed. To obtain the genuine Raman spectra of the as-synthesized materials, excitation energies smaller than the electronic band gaps of these compounds were used. For both Ca-Y/12.5Se and La-Y/13.5Se the band gap is approximately 2.35 eV which corresponds to photons of wavelength 525 nm.[15] Figure 1 shows the Raman

[⊗] Abstract published in *Advance ACS Abstracts,* January 1, 1997.

S1089-5647(96)02563-1

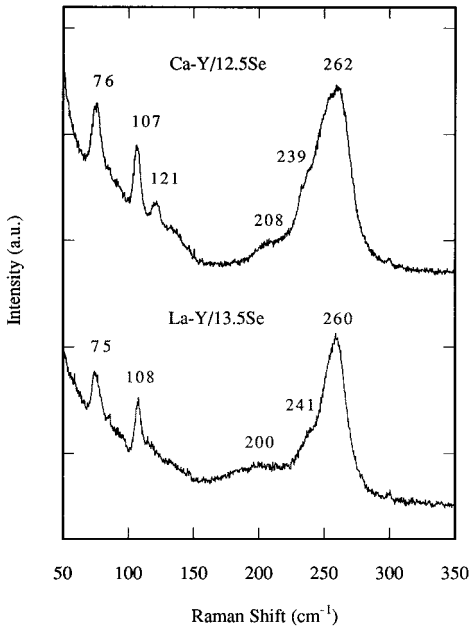

Figure 1. Raman spectra of La-Y loaded with 13.5 Se atoms (lower trace) and Ca-Y loaded with 12.5 Se atoms per supercage (upper trace), respectively. The excitation energy is 647.1 nm at an laser output of 20 mW.

spectra of both compounds at an excitation energy of 1.92 eV (647 nm) and 20 mW laser output. Both spectra can be divided roughly into two regions. In the region below 150 cm^{-1} two clearly distinguishable peaks at 75 and 108 cm^{-1} are superimposed on a background which increases steadily towards lower frequencies. The region above 150 cm^{-1} is dominated by a rather broad band near 260 cm^{-1}. This band is accompanied by a shoulder around 240 cm^{-1}, and a very broad and weak band around 200 cm^{-1}. No bands could be detected beyond 300 cm^{-1}, and the spectra do not change with time under these illumination conditions. The spectra resemble those of bulk amorphous and liquid Se.[16] The high-frequency bands are due to the transverse optical bond stretching modes of Se chains while the low-frequency band near 108 cm^{-1} is usually assigned to bond bending vibrations of ring like chain segments.[16]

This picture changes remarkably when we switch the laser to 476 nm (2.60 eV) now exciting well beyond the electronic gap of the encapsulated Se. A series of new bands above 300 cm^{-1} appear in the Raman spectra of both La-Y/13.5Se (Figure 2) and Ca-Y/12.5Se (Figure 3) while the low-frequency modes decrease in intensity. In addition, broad fluorescence bands are observed. As observed previously with Se incorporated into Nd-Y zeolite (Nd-Y/9.5Se),[1] the new bands grow slowly under continuous laser illumination. Simultaneously, the 260 cm^{-1} bands diminish and shift to higher frequencies and the stronger bands of the pure zeolites (Ca-Y 289, 527 cm^{-1}; La-Y 282, 515 cm^{-1})[15] become evident. To establish that these changes in the spectra are not due to heating of the laser beam, we recorded spectra as function of the laser power P. The spectra shown in Figures 2 and 3 have been recorded at $P = 8$ mW and $P = 20$ mW, respectively, but the new bands already develop at even lower laser output. To slow down the destruction of the originally encapsulated Se, the laser power at 476 nm has to be turned down to less than 1 mW. Furthermore, because of the reduced penetration depth at 476 nm the counting time has to be increased to 100 min as opposed to 5−10 min with 647 nm radiation and 20 mW. Despite the paucity of statistics of spectra recorded under these conditions, the La-Y/13.5Se spectrum shown in Figure 4 clearly reproduces the band at 260 cm^{-1}.

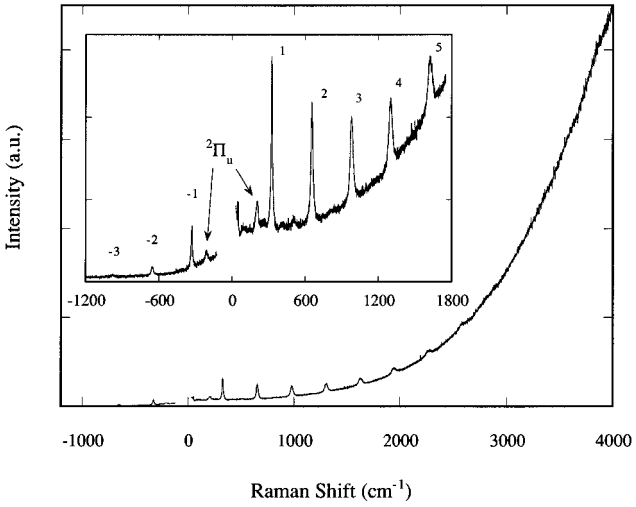

Figure 2. Raman spectrum of La-Y loaded with 13.5 Se atoms at an excitation wavelength of 476.2 nm ($P_{laser} = 8$ mW). The numbers denote the Stokes and anti-Stokes bands originating from Se_2^-. The bands at 210 and −207 cm^{-1} are due to scattering of Se_2^- in the excited $^2\Pi_u$ state.

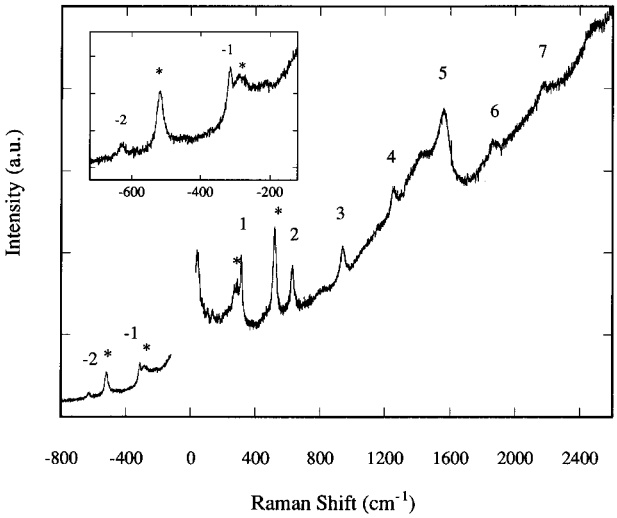

Figure 3. Raman spectrum of Ca-Y loaded with 12.5 Se atoms at an excitation wavelength of 476.2 nm ($P_{laser} = 20$ mW). The numbers denote the Stokes and anti-Stokes bands originating from Se_3. The asterisks mark vibrations of the Ca-Y zeolite framework. The broad peak around 1400 cm^{-1} is due to "hot fluorescence" of Se_3.

As in the case of Se encapsulated in Nd-Y zeolite, Se_2^- is formed in La-Y when excited at 476 nm. Figure 2 shows the corresponding resonance Raman spectrum ($P_{laser} = 8$ mW) which consists of a series of eight Stokes bands (Table 1) superimposed on a steeply rising broad fluorescence background. In addition, three anti-Stokes bands are detected on the high-energy side (Table 1). Standard analysis of the Stokes bands yields $\omega_0 = 329$ cm^{-1} and $\omega_0 x_0 = 0.8$ cm^{-1} in good agreement with the constants obtained for Se_2^- in Nd-Y: $\omega_0 = 328.5$ cm^{-1} and $\omega_0 x_0 = 0.7$ cm^{-1}.[1] Unlike in Nd-Y[1] the fluorescence background that accompanies the Se_2^- does not have a shoulder around 3500 cm^{-1} in La-Y. However, an additional Stokes and the corresponding anti-Stokes band can be recognized at 210 and −207 cm^{-1}, respectively. While the observed fluorescence in La-Y is probably ordinary luminescence of Se_2^- the additional fluorescence peak in Nd-Y is hot luminescence which is emitted from the excited vibrational levels populated in the course of vibrational relaxation of Se_2^- in the excited electronic state.[17] The 210 cm^{-1} band does not appear in Nd-Y/9.5Se upon illumination. This frequency does not correspond to a known

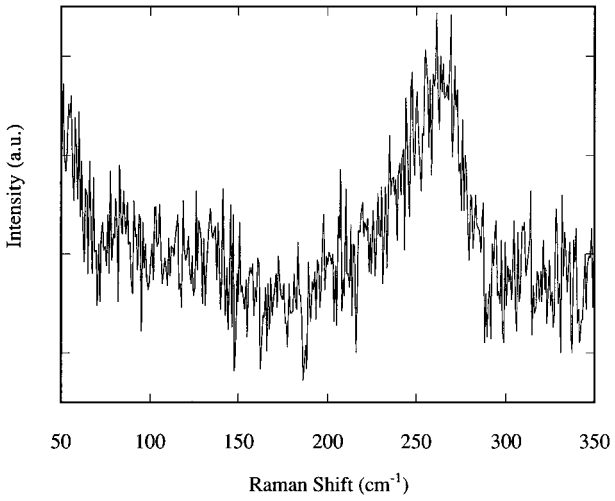

Figure 4. Raman spectrum of Ca-Y loaded with 12.5 Se atoms at an excitation wavelength of 476.2 nm and a laser output of 0.5 mW. Despite poor statistics even at increased counting time, the main features of the spectrum obtained at 647.1 nm and 20 mW can be recognized.

TABLE 1: Resonance Raman Bands of Se_3 in Ca-Y and of Se_2^- in Nd-Y[1] and La-Y

band no.	Nd-Y/9.5Se (cm^{-1})	La-Y/13.5Se (cm^{-1})	Ca-Y/12.5Se (cm^{-1})
1	328.0	327.2	315.0
2	656.8	654.0	628.0
3	981.8	979.7	942.5
4	1306.4	1303.6	1254.0
5	1625.8	1624.9	1558.0
6	1947.3	1944.9	1874.0
7	2268.2	2268.8	2172.0
8	2585.3	(2578.5)	
9	2900.9		
10	3219.3		
−1		−328.4	−313.5
−2		−654.1	−637.0
−3		−979.6	

vibration of any plausible molecular or extended cluster structure of neutral or ionic forms of selenium. However, the value itself comes close to the vibrational constant $\omega_0 = 216$ cm^{-1} of the $^{80}Se_2^-$ excited electronic $^2\Pi_u$ state that is involved in the resonance process.[18]

Differences in the Raman spectra of Se_2^- in La-Y and Nd-Y can be understood by taking into account the results of Murata et al., who studied the photoluminescence of Se_2^- implanted in a KI crystal.[19] The lifetime of the ordinary luminescence was reported as $\tau_R = 85$ ns at 2 K and remained constant up to 40 K. Although τ_R decreases rapidly above 60 K, an extrapolation of the decay curve suggests a lifetime long enough to allow Raman scattering from the Se_2^- $^2\Pi_u$ state in KI at room temperature ($\omega_0 = 216$ $cm^{-1} \rightarrow \nu = 6.5 \times 10^{12}$ s^{-1}). Assuming a thermally activated decay, they derived an activation energy of $\Delta E = 53$ meV (427 cm^{-1}) which is about twice as large as the fundamental vibrational energy of Se_2^- in the $^2\Pi_u$ state. Murata et al. concluded that another electronic state is intersecting the $^2\Pi_u$ state near the second vibrational level. Thus an intersystem crossing is feasible leading to the population of a state ($^2\Sigma_g^+$) which gives rise to a nonradiative decay to the $^2\Pi_g$ ground state. Also, the decay of the $^2\Pi_u$ state is paralleled by a drop in intensity of the ordinary luminescence.

The situation of Se_2^- in La-Y and Nd-Y may not be too different from that in KI since coupling of the ion to the matrix is weak. The scheme outlined in the previous paragraph would account for the additional bands at 210 and −207 cm^{-1} and the missing hot luminescence in the La-Y/13.5Se spectrum as well as the relatively weak Se_2^- resonance Raman bands compared to Nd-Y/9.5Se. The higher laser output in our earlier study (40−100 mW) might have been sufficient to promote a fast intersystem crossing preventing an efficient trapping of Se_2^- in the $^2\Pi_u$ state. At the same time the ordinary fluorescence will be largely quenched and, as observed, the resonant Raman bands and the hot luminescence of the Se_2^- become more prominent in the Nd-Y/9.5Se spectrum. On the other hand, the quenching of the Se_2^- $^2\Pi_u$ state in Nd-Y zeolite also could be caused by the presence of the paramagnetic Nd^{3+} ion since the UV/vis spectrum of the pure Nd-Y zeolite[15] shows several electronic bands in the visible and near-infrared region. Coupling between the Se_2^- $^2\Pi_u$ state and a Nd^{3+} excited state is another conceivable route for the fast removal of excited radical anions.

The spectrum of Ca-Y/12.5Se displayed in Figure 3 has been recorded at a laser output of 20 mW. Again a progression of eight Stokes bands (marked with numbers, see also Table 1) can be distinguished from an underlying fluorescence background. In addition, two anti-Stokes bands (Table 1) are found on the high-energy side of the excitation wavelength. Also both Stokes (slightly shifted) and anti-Stokes bands of the Ca-Y at 295, 518, −295, and −515 cm^{-1} become evident. The fluorescence background rises steadily toward lower energies with an additional peak at 1400 cm^{-1}. Analysis of the overtone wavenumbers yields values of $\omega_0 = 315$ cm^{-1} and $\omega_0 x_0 = 0.5$ cm^{-1} for the progression of Stokes bands. These values are in reasonable agreement with those found by resonance Raman scattering on Se_3 isolated in an argon matrix, yielding $\omega_0 = 312.15$ cm^{-1} and $\omega_0 x_0 = 0.53$ cm^{-1} for $^{80}Se_3$.[20] Our assignment of the resonance Raman bands to Se_3 is also substantiated by the fluorescence spectrum. The fluorescence peak at 1400 cm^{-1} corresponds to an absolute energy of 2.43 eV or $\lambda = 510$ nm and coincides with a broad absorption band obtained in a second matrix isolation study and assigned to Se_3.[21] Presumably the 1400 cm^{-1} peak arises from hot luminescence since the ordinary luminescence band of Se_3 is located between 684 nm and 842 nm.[20] The existence of an additional feature in the luminescence spectrum also explains the enhanced intensity of the fourth overtone at $\omega_4 = 1570$ cm^{-1} (labeled 5 in Figure 3). Since this overtone has an energy close to that of the luminescence at 1400 cm^{-1} there is an additional enhancement of this band due to the energy denominator in its cross section.

The progressive broadening of the bands at higher wavenumbers reflects the larger spread in energy of transitions arising from molecules with different isotopic composition. Natural Se consists of six isotopes with ^{80}Se (49.8%) and ^{78}Se (23.5%) being most abundant. While there are already 21 isotopic combinations for Se_2^-, the mixture of Se_3 consists of 56 molecules differing in their physical properties. Hence, the above-derived spectroscopic constants are average values for a large number of different species.

Figure 5 shows the low-frequency range of the Se_3 Raman spectrum on the Stokes side of the excitation wavelength. Weak features can be distinguished at 108, 137, 177, and 274 cm^{-1}. Clearly the dominant band at 262 cm^{-1} in the original material has almost vanished (Figure 1). While the feature at 177 cm^{-1} can be attributed to the zeolite host, it is likely that the other modes characterize at least one more remnant of the obliterated Se chains initially formed in the zeolite. In this respect it is interesting that Poborchii recently revised the interpretation of the polarized Raman spectra of Se loaded into mordenite taking into consideration the spectra of a mordenite/sulfur encapsulate.[9] He suggested that bands at 104, 135, and 274 cm^{-1} point to Se_6 rings confined in the one-dimensional channels of mordenite.

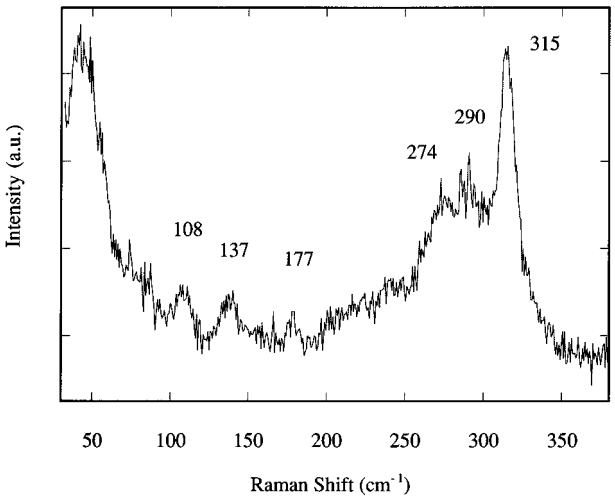

Figure 5. Details from the Raman spectrum of Ca-Y loaded with 12.5 Se atoms at an excitation wavelength of 476.2 nm (P_{laser} = 20 mW).

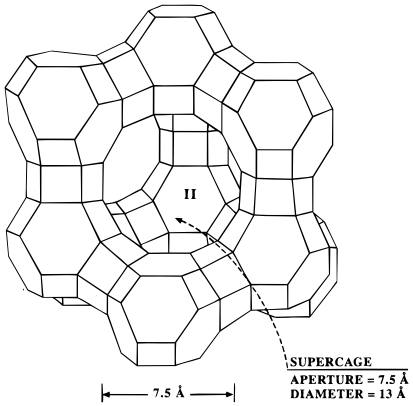

Figure 6. Schematic drawing of the supercage of zeolite Y.

Although these channels are hardly wide enough (6.7 Å) to squeeze in the Se_6 ring (6.5 Å) the conclusion that these modes should be attributed to a ring molecule is convincing. However, the generation of Se_3 in Ca-Y under 476 nm radiation appears to be accompanied by the formation of a secondary, probably ringlike, Se species.

Discussion

The two different Se molecules obtained from the photoinduced decomposition of Se adsorbed into La-Y and Ca-Y demonstrate the important role of the countercations in this reaction. The unit cell of Y zeolites contains eight of the supercages depicted in Figure 6. These cages measure 13 Å in diameter and are interconnected through four tetrahedrally arranged windows of 7.5 Å width. Apart from these large cages, the framework embodies also sodalite cages of 6.5 Å width with eight 2.2 Å wide hexagonal windows. Half of these windows are directed toward the hexagonal prisms which interconnect the sodalite cages, the rest toward the supercages. Charge balance in our zeolites requires 57 cationic charge equivalents per unit cell. For the samples exchanged with Nd^{3+} and La^{3+}, all the rare-earth ions are located in the small sodalite cages of the FAU structure and are not readily accessible for bonding to Se species in the supercage. However, for samples exchanged with divalent or monovalent cations the number of cations per unit cell exceeds the capacity of the sodalite cages. Some of the countercations are then located in exposed sites in the supercages. In particular, approximately 40% of the cations in the case of dehydrated Ca-Y zeolite (≈11.4 cations per unit cell) are located in Type II sites on the 3-fold axis near the six-rings defining the passage from the supercage to the sodalite cage. This corresponds to an average of 1.4 Ca^{2+} cations per supercage in the four available sites. These ions are available for bonding or complexation with Se species in the supercages.

The change to La does not alter the general picture obtained for Nd-Y in our previous study. Again we observe an extensive degradation of the initially encapsulated Se chain leading to the formation of Se_2^-. In contrast, this radical anion has not been detected in Ca-Y. The hydroxyl-bridged metal clusters clearly play a crucial role in the generation of Se_2^- in Y zeolite. Since the $M_xO_y(OH)_z^{n+}$ clusters (M = Nd, La) are located in the sodalite cages a stabilization of the Se_2^- via direct interaction is unlikely because the Se chain precursor in the supercage cannot enter the sodalite cages through the small hexagonal windows. Therefore, the main function of these clusters must be that of an electron source reducing one of the primary products formed in the photolytic reaction and thus preventing the fragments from immediate recombination. In the absence of an effective reducing agent a neutral species, Se_3, is formed in Ca-Y although the Ca^{2+} ions in Type II positions present now an anchor site for anions in the supercage. If the stabilization of negatively charged species was merely due to Coulombic type of interactions, cations in the supercage should have an even stronger effect. Thus, the failure of Se_2^- anions to be stabilized in the Ca-Y zeolite sample is seen as circumstantial evidence that the presence of the hydroxyl-bridged cationic clusters in rare earth Y-zeolites is necessary for the formation of the Se_2^- species.

On the other hand, the stabilization of Se_3 can be rationalized in terms of Coulomb interactions with the Ca^{2+} ions in the Type II positions. The matrix isolation studies as well as molecular dynamics calculations show the ground state structure of Se_3 to be the open C_{2v} structure corresponding to that of the homologous ozone O_3.[20,22] Like the D_{3h} ring—a second, nearly degenerate low-energy structure—the C_{2v} structure has a singlet ground state. The Se−Se bond distance in the open isomer indicates a bond order between one and two[22] pointing to a highly polarized mesomeric structure: The center atom carries a partial positive charge while each end atom carries a partial negative charge. Thus, Se_3 can act like a chelate ligand making a bidental coordination to the Ca^{2+} in the supercages. Cations in Type II sites are exposed and readily coordinate ligands in the supercage.

In contrast with our well-defined picture of the Se_3 environment, the exact location of Se_2^- in the rare earth Y zeolites remains unclear. In selenium ultramarine, Se_2^- is believed to be in the center of the sodalite cages tetrahedrally surrounded by four Na^+ ions.[11] A similar arrangement can be ruled out for the rare earth faujasite. First, the Nd or La cluster ions will occupy a larger volume of the sodalite cages than isolated cations. Second, the precursor Se chains are in the supercages and a migration of neutral or charged chain fragments like Se_2^- through the small apertures of the sodalite cages is very unlikely. Even in the case of selenium ultramarine it is assumed that the aluminosilicate framework develops around Se_2^- or a precursor during synthesis resulting in its encapsulation in the sodalite cage.[11]

Conclusion

Electronic excitation of Se encapsulated in zeolite Y leads to dissociation of the Se chain structure initially formed inside the zeolite. The cations necessary to counterbalance the negative framework charges of zeolites have a profound impact on this photochemistry. While rare earth cluster cations favor the

formation of Se_2^-, in the case of the simple cation Ca^{2+}, neutral species like Se_3 and possibly Se_6 are the products detected by Raman scattering. The complexation of the Ca^{2+} ions in the large cages by Se_3 is proposed to account for the striking stability of this small cluster in Ca-Y.

The incorporation of photosensitive materials into zeolites and the subsequent photolytic decomposition of the encapsulate marks a new viable route for the synthesis and characterization of small clusters. This approach does not require the elaborate procedures associated with low-temperature noble gas matrices or molecular beam techniques. Also, zeolite matrices can stabilize both neutral and ionic species. Characterization of clusters is often marred by the inability to produce high concentrations of single-sized clusters. However, zeolites are highly selective matrices that may favor the formation of a single species as shown in the examples above. The manifold of zeolite structures and their simple modification by ion exchange provide a wide variety of matrices whose potential in stabilizing small clusters is hardly explored.

Acknowledgment. This work was supported by the U.S. Department of Energy, Division of Materials Sciences, Office of Basic Energy Sciences, under contract W-31-109-ENG-38. A.G. gratefully acknowledges a research grant from the Deutsche Forschungsgemeinschaft.

References and Notes

(1) Goldbach, A.; Iton, L.; Grimsditch, M.; Saboungi, M.-L. *J. Am. Chem. Soc.* **1996**, *118*, 2004.

(2) Katayama, Y.; Yao, M.; Ajiro, Y.; Inui, M.; Endo, H. *J. Phys. Soc. Jap.* **1989**, *58*, 1811.

(3) Endo, H.; Inui, M.; Yao, M.; Tamura, K.; Hoshino, H.; Katayama, Y.; Maruyama, K. *Z. Phys. Chem. N. F.* **1988**, *156*, 507.

(4) Bogomolov, V. N.; Poborchii, V. V.; Kholodkevich, S. V.; Shagin, S. I. *JETP Lett.* **1983**, *38*, 532.

(5) Bogomolov, V. N.; Poborchii, V. V.; Romanov, S. G.; Shagin, S. I. *J. Phys. C: Solid State Phys.* **1985**, *18*, L313.

(6) Bogomolov, V. N.; Poborchii, V. V.; Kholodkevich, S. V. *JETP Lett.* **1985**, *42*, 517.

(7) Bogomolov, V. N.; Efimov, A. N.; Ivanova, M. S.; Poborchii, V. V.; Romanov, S. G.; Smolin, Yu. I.; Shepelev, Yu. F. *Sov. Phys. Solid. State* **1992**, *34*, 916.

(8) Poborchii, V. V. *J. Phys. Chem. Solids* **1994**, *55*, 737.

(9) Poborchii, V. V. *Chem. Phys. Lett.* **1996** *251*, 230

(10) Clark, R. J. H.; Dines, T. J.; Kurmoo, M. *Inorg. Chem.* **1983**, *22*, 2766.

(11) Lindner, G. G.; Reinen, D. *Z. Anorg. Allg. Chem.* **1994**, *620*, 1321.

(12) Cheetham, A. K.; Eddy, M. M.; Thomas, J. M. *J. Chem. Soc., Chem. Commun.* **1984**, 1337.

(13) Brennan, D.; Catlow, C. R. A.; Jackson, R. A. *Zeolites* **1994**, *14*, 660.

(14) Bogomolov, V. N.; Kholodkevich, S. V.; Romanov, S. G.; Agroskin, L. S. *Solid State Comm.* **1983**, *47*, 181.

(15) Goldbach, A., unpublished results.

(16) Carroll, P. J.; Lannin, J. S. *J. Non-Cryst. Solids* **1980**, *35/36*, 1277.

(17) Rebane, L. A.; Khaldre, T. Yu. *JETP Lett.* **1977**, *26*, 515.

(18) Vella, G. J.; Rolfe, J. *J. Chem. Phys.* **1974**, *61*, 41.

(19) Murata, H.; Kishigami, T.; Kato, R. *J. Phys. Soc. Jpn.* **1990**, *59*, 506.

(20) Schnöckel, H.; Göcke, H.-J.; Elsper, R. *Z. Anorg. Allg. Chem.* **1982**, *494*, 78.

(21) Brabson, G. D.; Andrews, L. *J. Phys. Chem.* **1992**, *96*, 9172.

(22) Hohl, D.; Jones, R. O.; Car, R.; Parrinello, M. *Chem. Phys. Lett.* **1987**, *139*, 540.